High temperature conductance mapping for correlation of electrical properties with micron-sized chemical and microstructural features

Hansen, Karin Vels; Norrman, Kion; Jacobsen, Torben

Published in:
Ultramicroscopy

Link to article, DOI:
10.1016/j.ultramic.2016.07.019

Publication date:
2016

Document Version
Peer reviewed version

High temperature conductance mapping for correlation of electrical properties with micron-sized chemical and microstructural features.

Karin Vels Hansen [a*], Kion Norrman[a], Torben Jacobsen[b]

[a] Department of Energy Conversion and Storage, Technical University of Denmark, Frederiksborgvej 399, Roskilde, DK-4000 Roskilde, Denmark
[b] Department of Chemistry, Technical University of Denmark, Kemitorvet Building 207, DK-2800 Kgs. Lyngby, Denmark

*corresponding author: Karin Vels Hansen, karv@dtu.dk

Abstract

High temperature AC conductance mapping is a scanning probe technique for resolving local electrical properties in microscopic areas. It is especially suited for detecting poorly conducting phases and for ionically conducting materials such as those used in solid oxide electrochemical cells. Secondary silicate phases formed at the edge of lanthanum strontium manganite microelectrodes are used as an example for correlation of chemical, microstructural and electrical properties with a spatial resolution of 1–2 μm to demonstrate the technique. The measurements are performed in situ in a controlled atmosphere high temperature scanning probe microscope at 650 °C in air.

Keywords: high temperature scanning probe microscopy, in situ scanning probe microscopy, conductance, microelectrodes, secondary phases

1. Introduction

In situ and in operando techniques are increasing in number due to the need for assessing properties of functional materials while they are at work as compared to ex situ analyses where the conditions may deviate so much that it influences the properties to be determined. Many properties of solid oxide cell (SOC) materials cannot be investigated at room temperature due the temperature dependence of conductivity of the electrolyte and the electrocatalytic properties of the electrodes. Detailed investigation of degradation mechanisms of SOCs are difficult to perform in operando as the vital locations are inaccessible, and further, SOC electrodes have complicated three dimensional microstructures which are difficult to describe and quantify as they have a porous microstructure and consist of two or more phases. The triple phase boundaries (TPB) where the gas, electrode and electrolyte meet and where the electrochemical reactions take place are not visible or accessible and the TPB properties cannot easily be evaluated. Local measurements of the TPB may be performed in model systems such as microelectrodes where the simple geometry makes the accessibility easy and the calculation of parameters such as TPB length and surface and interface areas uncomplicated.

With scanning probe microscopy (SPM) such as a controlled atmosphere high temperature scanning probe microscope (CAHT-SPM) [1] microelectrodes and their TPB can be addressed individually, and local electrical or electrochemical properties can be measured in situ or in operando. The

CAHT-SPM was developed to study electrical properties of high temperature materials in controlled atmospheres and works in the temperature range of 25–850 °C and with in-house fabricated Pt-10 % Ir probes [2] which have good mechanical properties also at high temperature.
Electrical measurements used in scanning probe microscopy are abundant and comprise e.g. scanning tunneling microscopy and spectroscopy, Kelvin probe microscopy, conductive atomic force microscopy but also other techniques for measuring impedance, capacitance, resistance etc. have been reported [3]. The majority of literature on SPM concerns measurements at temperatures below ~200 °C and measurements at higher temperatures combined with a controlled atmosphere at atmospheric pressure are very limited, as recently reviewed by Nonnenmann [4]. With the CAHT-SPM we have developed a technique based on AC conductance measurements using a lock-in amplifier. This technique is ideal for conducting materials with relatively low conductances or poorly conducting phases. Conductance maps can be acquired quickly and simultaneously with topography images [1] and small inhomogeneities with a lateral extension of 1–2 microns can be revealed.
The present report explains the main principles of the conductance mapping technique and demonstrates how micron-sized features in the conductance images correlate well with features recorded by time-of-flight secondary ion mass spectrometry (TOF-SIMS) imaging and microstructural features observed in scanning electron microscopy (SEM) images thus validating the observations in the CAHT-SPM.
Previously, lanthanum strontium manganite (LSM) microelectrodes on yttria-stabilized zirconia (YSZ) were characterized by impedance spectroscopy and cyclic voltammetry in a CAHT-SPM [5], microstructurally by SEM [5] and chemically by TOF-SIMS [6]. Here they are used as an example to demonstrate the correlation between electrical, chemical and microstructural properties.

2. Materials and methods

2.1 Conductance mapping

The sample is mounted on the furnace of the CAHT-SPM (Figure 1) and kept in place by springs pressing the sample against the furnace. A platinum wire counter electrode is attached to the edge of the sample. A sine wave AC voltage is applied to the tip or the sample by the sine wave generator of a Stanford SR830 lock-in amplifier. The resulting current is measured by the lock-in amplifier through a 1 MΩ resistor for overload protection to avoid overload on samples with highly conducting regions. The current output of the lock-in amplifier is then directed to the external input option of the CAHT-SPM controller and depicted along with the topography during normal contact mode scanning. The conductance, $G=1/(R+1\ \mathrm{M\Omega})$ where R is the local sample resistance at the tip-sample contact, is calculated as the ratio of the in-phase current and the output voltage, and subsequently the conductance is corrected for value of the series resistor before plotting the data.
The conductance measurements are continuous single frequency measurements performed simultaneously with topography scans. Typically a voltage of 0.5 V rms at 10 kHz is used.
Mostly, the scan speed is chosen to record the scan width in a second, i.e. spending 8–4 ms per pixel depending on the resolution of 128 or 256 pixels per line. With a filter setting of 6 dB per ms and 10 kHz this results in a weighted average over 40–80 AC cycles. In practice, a complete

128×128 or 256×256 can be obtained in 10-20 min, i.e. a time that requires a highly stable system. But, as seen from Figure 2, the drift after the initial thermal equilibration is less than 50 nm per minute and the distortion of the image will therefore be negligible for scans covering more than a few μm^2.

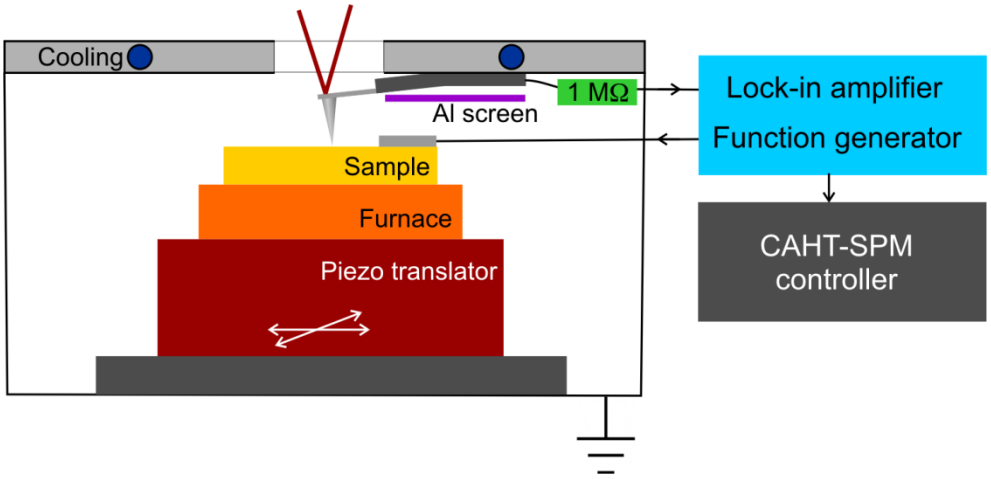

Figure 1. The set-up in the CAHT-SPM during conductance mapping. The aluminium screen (purple) minimizes stray capacitance between cantilever and sample.

With the present setup, experience indicates that the conductance can be determined in a range from a few nS up to ~100 μS, where the lower limit is determined by stray capacities shunting the probe-sample resistance. Due to the dimensions of the probes (~3x0.3 mm) and the probe holder the stray capacity is around 100 pF. It may be reduced further by a better screening, but this is not trivial due to the high temperature. Thus, it is not likely that the values in the aF range achieved [7, 8] at room temperature can be obtained. The upper limit is set by the 1 MΩ overload protection resistor. Although the final data are corrected for the resistor, the accuracy is reduced above ~10 μS.

In principle, the lower limit can be lowered further by reducing the frequency and in the case of measurements on electronic conductors the only condition is that of a few AC cycles per point in order to achieve a good resolution. However, on ionic conductors there is a shift from electronic conduction in the probe to the ionic conduction in the sample and either an electrochemical reaction resulting in an overvoltage at the probe-sample contact, or a capacitive shunt through the interfacial capacity is required. Therefore, the choice of frequency is a trade-off between the influence of the stray capacities and that of the probe-sample contact. In our measurements, mainly on oxide ion conductors, 10 kHz has proven a reasonable compromise.

When scanning a rather homogeneous sample, the conductance measured is crudely an average value of a volume close to the probe-sample contact point weighted with the reciprocal distance squared, i.e. only extending a few probe-sample contact radii into the sample. For inhomogeneous samples the situation is more complicated.

If, for example, the probe is contacting a thin microelectrode deposited on an ionic conductor, the electronic conductivity of the electrode material will normally exceed the ionic conductivity of the electrolyte by several orders of magnitude and the effective probe-sample contact area will be

extended significantly. If the lateral conductance is very high, the electrode itself will be the actual probe-sample contact and the conductance determined will follow the relation for a circular contact to a poorly conducting medium [9]: $G=4\cdot\sigma\cdot R$, where σ is the ionic conductivity and R the radius of the electrode. If the ratio between the electrode conductivity and the conductivity of the electrolyte is lowered, the current field at the electrode-electrolyte interface is confined to a minor area around the probe-electrode contact and the spatial conductance resolution is improved. Figure 3. shows the result of finite element calculations of normalized conductances on a microelectrode with specified dimension as a function of the ratio between the electrode and the electrolyte conductivity. In the examples presented in this paper the ratio is: $\sigma_{LSM}/\sigma_{YSZ}=30/0.001 = 3\cdot10^3$ [10, 11], i.e. the effective contact radius is around 75 % of that of a microelectrode with a diameter of 100 μm.

Finally, as pointed out by Huber et al. [12] there may be a substantial cooling of the sample in the vicinity of the probe-sample contact. The effect depends on the physical contact area and may according to our calculations be less than 70 °C in stationary measurements with a physical contact area having a radius of 100 nm. During scanning the cooling will be somewhat lower but, still it is one of the factors that make an absolute interpretation of conductance scans difficult.

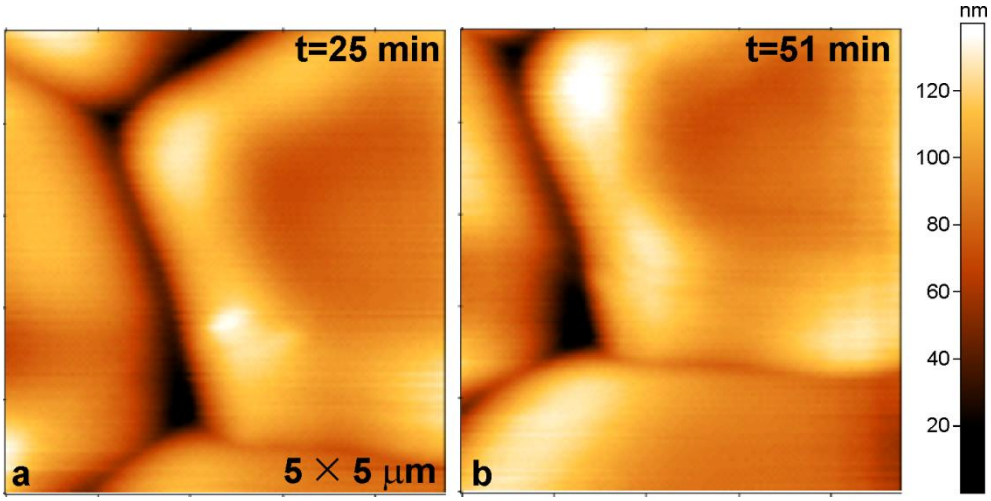

Figure 2. Drift study of polished and heat treated zirconia with an in-house made PtIr probe. The sample temperature is 600 °C, the scan speed is 5 μm/s. Time, *t*, is counted from when the sample reached 600 °C. Over 26 minutes the drift is less than 1 μm in both the x- and y-direction.

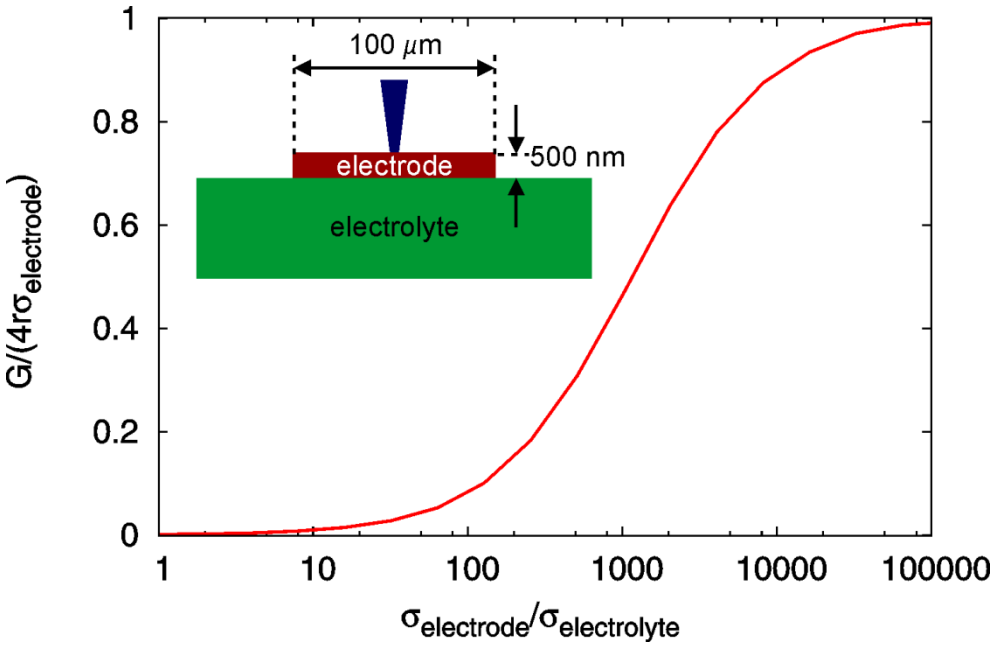

Figure 3. Conductance measured with the probe in the center of a circular thin-film microelectrode deposited on a substrate as function of the conductivity of the electrode material relative to that of the substrate. The conductance is normalized with the value corresponding to an infinite ratio. The graph is the result of finite element calculations using the FreeFem++ program [13].

2.2 Sample preparation

The microelectrodes were prepared by depositing 500 nm LSM $(La_{0.85}Sr_{0.15})_{0.95}MnO_3$ on a polished polycrystalline YSZ disk and performing photolithography and chemical etching, leaving microelectrodes of 20, 50 and 100 μm diameter in the center of the disk. The microelectrodes were subsequently sintered for 5 h at 1000 °C in air [5]. SEM and atomic force microscopy (AFM) images (Figure 4) of the as-sintered microelectrodes show the formation of particles with a different morphology at the edge of the microelectrodes and otherwise a uniform microelectrode surface of fine-grained LSM.

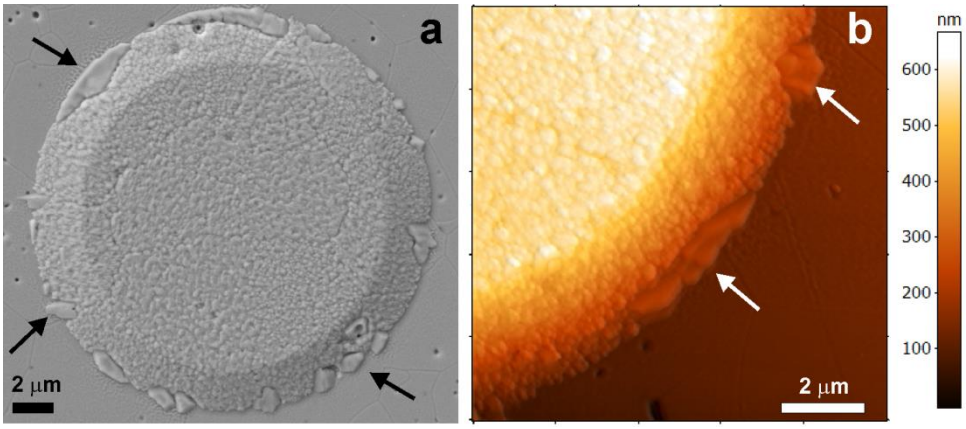

Figure 4. Secondary phases at the electrode circumference. a) SEM (SE) image of a microelectrode with a diameter of 20 μm. b) AFM topography image.

3. Results

3.1 Example 1: Correlation of conductance with chemistry and microstructure of as-sintered LSM microelectrodes

Figure 5 shows conductance images of different microelectrodes. The conductance of the as-sintered microelectrodes is high and uniform on the electrode surface as seen for microelectrodes with 100, 50 and 20 μm diameters (Figure 5a-c). In Figure 5c and d the edge of the microelectrode does not seem to be a perfect circle, and in a more detailed scan (Figure 5d) of the edge of the microelectrode in Figure 5 (red box) it is clear that a particle with a low conductance is present at the edge. This is also observed for the microelectrodes with 50 and 100 μm diameters, but in Figure 5a and b the scale is too large for such details to be obvious.

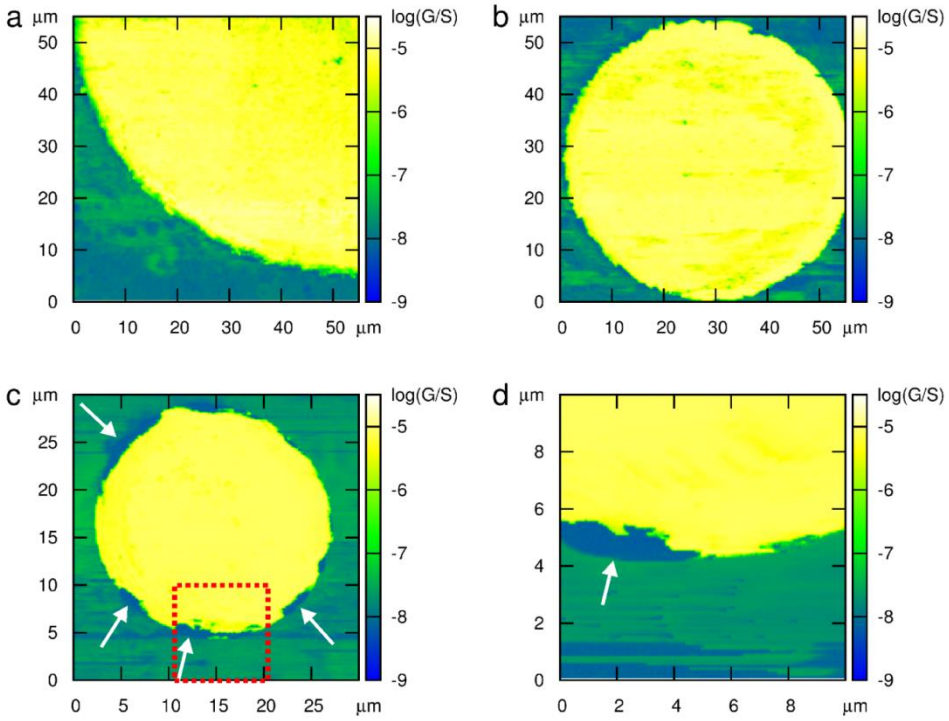

Figure 5. Conductance images obtained at 650 °C in air of a) Part of a microelectrode with a diameter of 100 μm, obtained with a scan speed of 55 μm/s and 128×128 points. b) Microelectrode with a diameter of 50 μm obtained with a scan speed of 55 μm/s and 256×256 points. c) Microelectrode with a diameter of 20 μm obtained with a scan speed of 30 μm/s. d) Part of the microelectrode in (c, red box), 10×10 μm scan with a scan speed of 10 μm/s. All images show a uniform and high conductance of the electrode area. Arrows point to poorly conducting phases at the microelectrode edge.

Detailed images of the edge of microelectrode with a diameter of 20 μm are presented in Figure 6. The conductance map in Figure 6a displays a very irregular edge of the high conductance area and Figure 6b shows an even more detailed image of this region. Figure 6c and d show a SEM image

and a topography image corresponding to Figure 6b. Clearly the circumferences are not coinciding and where the conductance image shows the edge of the high conductance area curving inward, the topography shows the edge is curving outward. The conductance images thus show that the secondary phase located at the TPB/circumference has a poor conductance and cannot be pure LSM. The same correlation can be observed for the 50 and 100 µm electrodes (not shown). Figure 7 shows a direct correlation between a conductance image (Figure 7a) and an SEM image (Figure 7b). In the topography image (Figure 7c the topography image is found to agree with the SEM image on the circumference of the microelectrode.

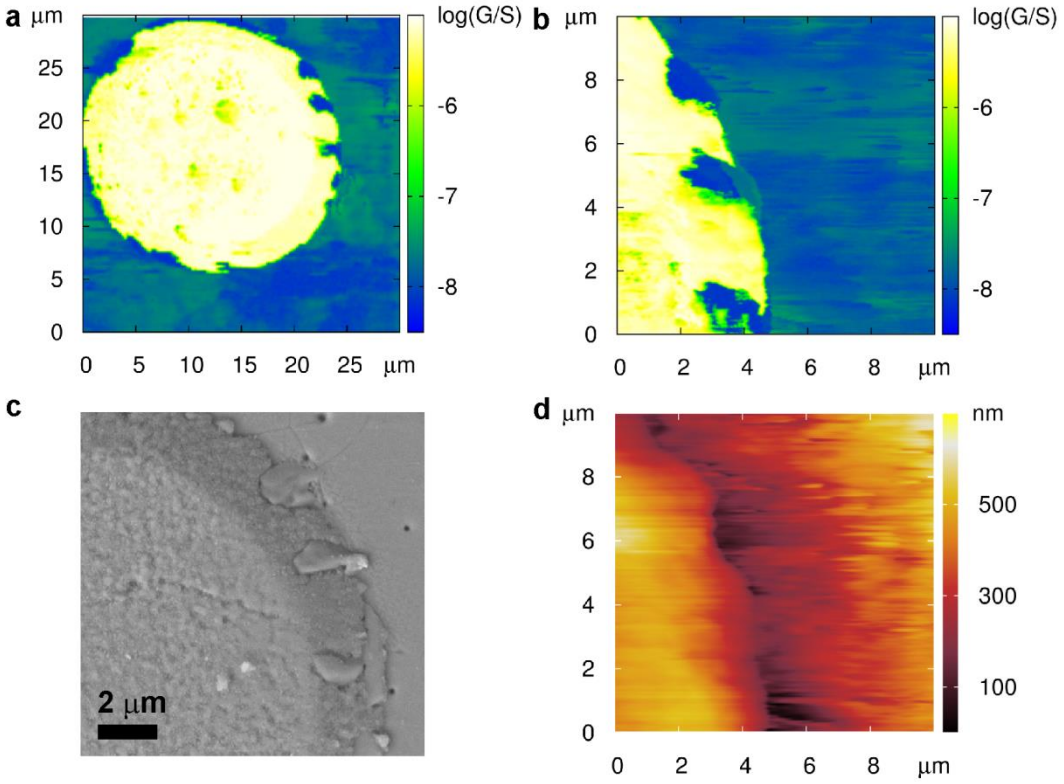

Figure 6. a) Conductance images of a microelectrode with a diameter of 20 µm obtained at 650 °C in air. b) Detailed conductance image of a part of (a). c) SEM (SE) image of the same area and d) topography corresponding to b).

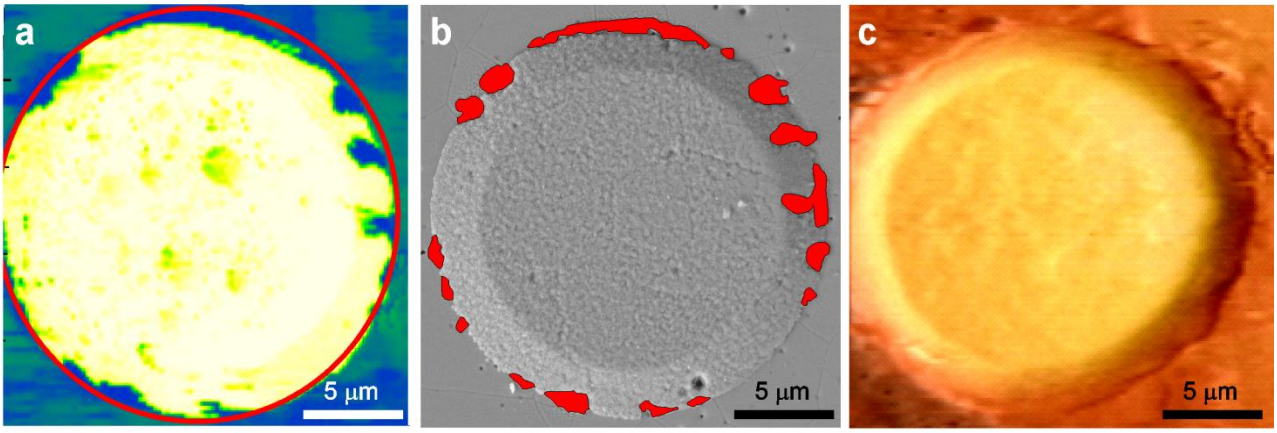

Figure 7. a) Conductance map of the microelectrode from Figure 6 with a circle at the microelectrode circumference to guide the eye and b) SEM (SE) image of the same microelectrode with the secondary phases marked in red. c) High temperature topography image.

TOF-SIMS imaging of the microelectrodes also clarifies the secondary phases as being different from the LSM. Figure 8 shows TOF-SIMS images of selected elements, and the irregular circumference is obvious in the Si (Figure 8a) and Mn (Figure 8b) ion images as well as in the composite (Figure 8d) ion image. The Zr ion image shows that the microelectrode edge is smooth and that zirconia is not a part of the secondary phase. Figure 8d shows a composite image of La, Mn, and Si where it is clear that La and Si are one of the main components of the secondary phase.

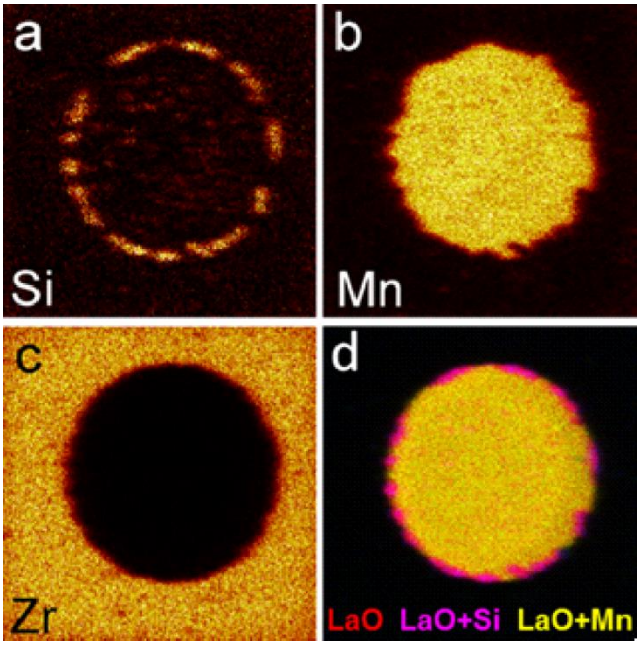

Figure 8. TOF-SIMS images of a microelectrode with a diameter of 20 µm. The primary ion conditions were 100 fA of Bi^+ with a lateral resolution of 200 nm and a probe depth of 1–2 nm. a–c) Si, Mn and Zr ion images. Bright colors indicate high intensities. d) Composite ion image of La, Mn, and Si.

3.2 Example 2: Correlation of conductance with chemistry and microstructure of microelectrodes exposed to high temperature for 200 h

After 200 h at elevated temperature the conductance of the microelectrode surfaces was not uniform anymore. Figure 9 shows conductance images of several microelectrodes obtained after they were exposed to 850 °C for 200 h. Figure 9a and b display images of the same microelectrode. Figure 9a is scaled to cover the entire experimental range, whereas the low conductance region is expanded in Figure 9b. The electrode surface shows areas of high conductance and low conductance and especially toward the edge it is found that the conductance is high only spot wise. The edge shows up as a wide rim with a very low conductance, even lower than that of the YSZ substrate. Figure 9c shows another microelectrode with the same features. The large blue-green area in the microelectrode surface Figure 9a is a fracture, where the electrode surface was torn out when the probe was lifted after contact during electrochemical characterization and the color shows that the underlying YSZ is exposed. Figure 9d shows a very detailed image of the edge where microstructural features can be distinguished.

SEM images of the edge region show that the outer 2–3 μm of the microelectrode edge have a microstructure that is significantly different from the as-sintered microelectrodes, and also that it is different from the electrode surface (Figure 10a). From Figure 10b, which shows a TOF-SIMS ion image of the Mn distribution at the microelectrode edge, it is clear that the edge does not consist of LSM. It consists of a phase with different chemical composition, has a different appearance and has a very low conductance (Figure 10c). The chemical composition of the microelectrodes was reported previously [6] and it was shown that the edge consists of a La-Sr silicate.

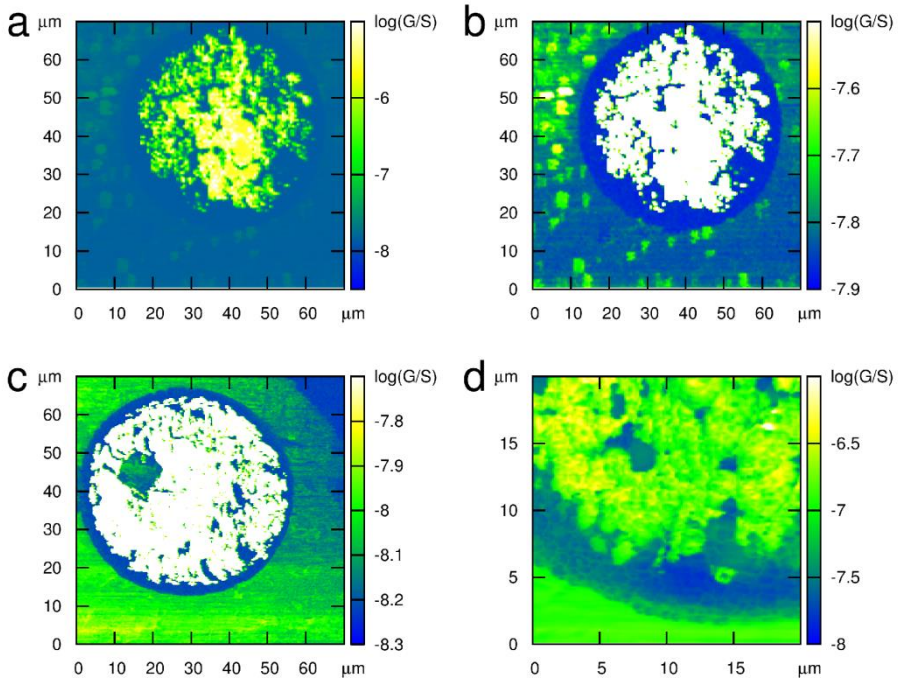

Figure 9. Conductance images obtained at 650 °C in air of microelectrodes with a diameter of 50 μm (a) and with a z-scale enhancing the low conductance region. c) A similar microelectrode. The arrow marks where a piece of the LSM was torn out, exposing the YSZ below. d) 20×20 μm scan of the edge of a microelectrode with a diameter of 50 μm.

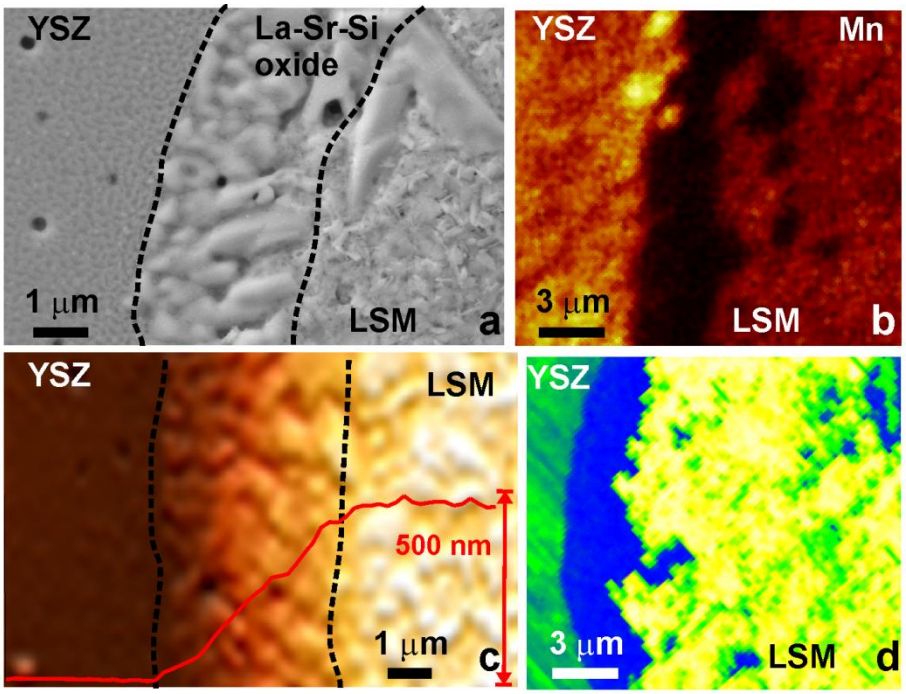

Figure 10. a) SEM (SE) images the microelectrode edge. b) TOF-SIMS Mn ion image of a similar microelectrode edge. Bright colors indicate high intensity of Mn. c) Room temperature topography image of the edge region of a similar microelectrode. The red curve shows the height profile. d) Conductance image of a similar microelectrode edge. Yellow indicates high and blue indicates low conductance.

3.3 Effects of scanning

TOF-SIMS imaging performed after conductance mapping shows that care must be taken regarding how many scans can be made without modifying the surface chemistry. Sr and Si ion images are shown in Figure 11 for a microelectrode with a diameter of 20 μm, and it is clearly seen that the scanning has caused Sr to be smeared outside the microelectrode area. These microelectrodes were scanned with a relatively high force set-point but it is probably equally important how many times the microelectrodes were scanned as it was not observed for all microelectrodes. The entire scan area is covered by La, Sr and Mn, which are then covering the segregated Si (Figure 11b). TOF-SIMS is an extremely surface sensitive technique analyzing only the outer 1–2 nm and since the Si is still visible below the Sr, it is not completely covering the surface. Such a thin layer of Sr does not necessarily affect the conductance measurements due to the larger probe depth.

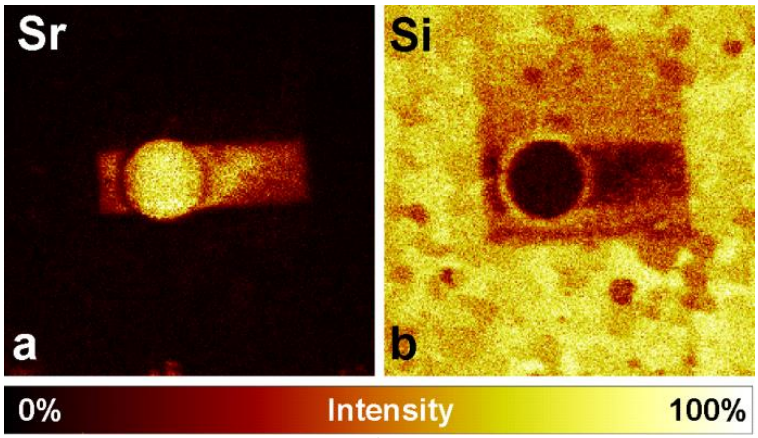

Figure 11. TOF-SIMS ion images (100×100 μm^2) of a microelectrode with a diameter of 20 μm. The primary ion conditions were 100 fA of Bi^+ with a lateral resolution of 200 nm and a probe depth of 1–2 nm. a) Sr contamination of the scanned area has occurred as a result of scanning. b) Sr is partly covering the Si which has segregated to the surface during heat treatment.

4. Discussion

The detailed investigation of LSM microelectrodes on YSZ shows a direct correlation between microstructural features, their chemical composition and conductance. The secondary phases in the as sintered microelectrodes located as particles up to a couple of micrometers in size at the microelectrode edge clearly show up as being different from the LSM. Measurements of local electrical properties of microscale features such as the secondary phases require a technique that is able to access the individual features. Scanning probe microscopy is well suited for this as the tiny probe size allows measurement in selected areas. However, for the results to be representative of the actual materials properties when they are working in their usual environment, it is necessary to perform the measurements under in operando or at least in situ conditions.

High-resolution in situ experiments is challenging due to the need for thermal stability to acquire high quality images. Thermal drift of the CAHT-SPM is less than 1 μm in x and y directions at 600 °C over a period of 26 minutes. It is thus possible to acquire images of sufficient quality if the scan speed is not too slow. In fact, there does not seem to be a resolution gain from decreasing the scan speed further. Another and more important factor is the force and the interaction between the probe and the sample. Experience shows that the force needed to keep the probe in contact with the sample typically increases with temperatures. As our in-house fabricated probes are solid metal they do not become less conducting with time unless the tip is contaminated but wear does occur and the tip becomes less sharp with time as with all contact mode measurements.

Conductance mapping is a robust and useful technique for investigation of local electrical properties of small features in their natural high temperature working environment. This is especially true for SOC materials. The resolution in the present study is found to be in the order of 1 – 2 μm and is probably mainly a function of the tip size.

5. Conclusion

Despite a number of factors such as cooling and uncertainty about tip size/contact area that complicate absolute measurements conductance mapping provides detailed qualitative information of electrical surface properties.

The conductance mapping technique allows a detailed study of areas of low conductance or phases and a correlation with morphological and chemical features for identification of their electrical properties in relation to the materials performance during in operando conditions.

Acknowledgment

We gratefully acknowledge financial support from Energinet.dk through the ForskEL programme "Solid Oxide Fuel Cells for the Renewable Energy Transition" contract no 2014-1-12231

References

[1] K. V. Hansen, Y. Wu, T. Jacobsen, M. B. Mogensen, and L. Theil Kuhn, Improved controlled atmosphere high temperature scanning probe microscope, Rev. Sci. Instrum., 84, 073701-073701-7 (2013).

[2] Y. Wu, K. V. Hansen, T. Jacobsen, and M. Mogensen, Impedance measurements on Au microelectrodes using controlled atmosphere high temperature scanning probe microscope, Solid State Ionics, 197, 32-36 (2011).

[3] S. V. Kalinin and A. Gruverman, *Scanning probe microscopy: Electrical and electromechanical phenomena at the nanoscale*, Springer, (2007).

[4] S. S. Nonnenmann, A hot tip: Imaging phenomena using in situ multi-stimulus probes at high temperatures, Nanoscale, 8, 3164-3180 (2016).

[5] K. V. Hansen, K. Norrman, T. Jacobsen, Y. Wu, and M. B. Mogensen, LSM microelectrodes: Kinetics and surface composition, J Electrochem. Soc., 162, F1165-F1174 (2015).

[6] K. Norrman, K. V. Hansen, T. Jacobsen, and M. B. Mogensen, Dynamic behavior of impurities and native components in model LSM microelectrodes on YSZ, RSC Adv., 5, 87679-87693 (2015).

[7] L. Fumagalli, G. Ferrari, M. Sampietro, and G. Gomila, Quantitative nanoscale dielectric microscopy of single-layer supported biomembranes, Nano Lett., 9, 1604-1608 (2009).

[8] L. Fumagalli, G. Ferrari, M. Sampietro, and G. Gomila, Dielectric-constant measurement of thin insulating films at low frequency by nanoscale capacitance microscopy, Appl. Phys. Lett., 91, 243110 (2007).

[9] R. Holm, *Stationary Contacts*, 4th edn., p. 16, Springer-Verlag, Berlin (1967).

[10] M. Marinsek, Electrical conductivity of sintered LSM ceramics, Materials and Technology, 43, 79-84 (2009).

[11] C. C. Appel, N. Bonanos, A. Horsewell, and S. Linderoth, Ageing behaviour of zirconia stabilised by yttria and manganese oxide, J. Mater. Sci., 36, 4493-4501 (2001).

[12] T. M. Huber, A. Opitz, M. Kubicek, H. Hutter, and J. Fleig, Temperature gradients in microelectrode measurements: relevance and solutions for studies of SOFC electrode materials, Solid State Ionics, 268, 82-93 (2014).

[13] F. Hecht, New development in freefem++, J. Numer. Math., 20, 251-265 (2012).